

Comparative study on the characteristics of ball-milled coal fly ash

Hui Li^{1,2,3} · Ying Chen³ · Yan Cao³ · Guijian Liu² · Buqing Li¹

Received: 29 August 2015 / Accepted: 12 November 2015 / Published online: 10 December 2015
© Akadémiai Kiadó, Budapest, Hungary 2015

Abstract High-energy mill (HEM) has a wide application in material preparation, activation and synthesis. In the present study, fly ash was selected to be milled by HEM under the speed of 700 rpm and the ball-to-powder ratio of 10:1 by weight, but varied periods of milling time. The changes in physical and morphology properties of the milled fly ash were determined using BET analysis and scanning electron microscope, those of chemical properties were determined using X-ray diffraction, mercury intrusion porosimetry and Fourier transform infrared, and their thermal properties were determined using thermogravimetric analysis (TG). The obtained data implied that the ball-milling treatment leads to reductions in both particle size and crystallite size of the milled fly ash, and also changes of their microstructural and functional groups, and loss of crystallinity. The milling time was found an important factor to impact extent of those changes. The large particles of the original fly ash regularly in an average of 5 μm were significantly broken down to much smaller particles (average diameter 300 nm), and the pore size distribution was also greatly changed by the ball-milling treatment and shown a close relevant to the milling time. Both patterns from FTIR and TG indicated the decrease in

intensity of –OH stretching vibration peak and increase in peak widths of the ball-milled fly ash with the increase in the ball-milling time, implying along ball-milling time leading the ball-milled fly ash toward more amorphousness and likely the higher reactivity.

Keywords Fly ash · Ball mill · XRD · FTIR

Introduction

Nanomaterials have drawn much attention due to their enhanced physical and chemical properties that are not shown in conventional materials. A large variety of methods have been developed to produce nanomaterials, which include the plasma arcing, the chemical vapor depositions, the electrodepositions, the sol–gel synthesis and the ball milling. In the majority of these approaches, the ball mill, with the benefits of time saving, process simplicity, cost reduction and solvent-free reaction condition [1, 2], can be easily scaled up to commercial levels of application. High-energy mill (HEM) has been specially attention to a wide application in material preparation, activation and synthesis [3, 4].

Fly ash is produced about 780 billion [5] tons every year worldwide from the huge amount of coal consumption. It has been considered to be the sixth most abandoned mineral in the USA and the world's fifth largest raw material resource [6–8]. Worldwide, most of the fly ash is land filled, leading to land occupation and potential environmental problems. Currently only small proportion (15–20 %) is reused as cheap construction materials, such as construction bricks, road fillers, and soil amendments [9–13]. Fly ash is heterogeneous power main including glassy and amorphous structure derived from inorganic,

✉ Yan Cao
yan.cao@wku.edu

¹ Agricultural Engineering Research Institute, Anhui Academy of Agricultural Sciences, Hefei 230031, Anhui, China

² CAS Key Laboratory of Crust-Mantle Materials and Environment, School of Earth and Space Sciences, University of Science and Technology of China, Hefei 230026, Anhui, China

³ Institute for Combustion Science and Environmental Technology, Western Kentucky University, Bowling Green, KY 42101, USA

incombustible matter present in coal. The chemical and physical characteristics of coal fly ash vary considerably with different combustion conditions, such as the coal properties, originalities of ash in coal, the boiler designs and combustion parameters. For this reason, the application of fly ash is more complicated [14–18]. It has been studied that the milled fly ash can cause an increase in the surface area and improve the pozzolanic activity, which can be used as adsorbent, cement, immobilization, etc. [19, 20].

In this work, an attempt has been made to modify coal fly ash by a high-energy ball milling at the speed of 700 rpm under varied periods of milling time. The milled ash samples were characterized by their physical and chemical properties using BET analysis, X-ray diffraction (XRD), thermogravimetric analysis (TG), scanning electron microscopy (SEM), Fourier transform infrared spectroscopy (FTIR) and mercury intrusion porosimetry (MIP).

Experimental methods

Fly ash samples used in this study were produced from a thermal coal power plant. Mechanochemical experiment of raw fly ash was carried out by a high-energy pulverization ball milling (Premium line, FRISCH, Germany) in an air atmosphere with a rotation speed of 700 rpm. The balls and grinding bowl used in the experiments were made of agate and stainless steel. The ball mill was loaded with 10:1 (mass ratio) for the ball (10 mm ϕ) and the sample. To avoid the generation of high temperature from high-speed ball mill, the milling time was set to 2-min working with 7-min breaks. To determine the effect of the ball-milling time, the total duration of milling process varies from 100 to 4000 min.

Thermogravimetric evaluations of all the samples were performed by TA100 under an inert nitrogen (99.99 % purity) atmosphere at a flow rate of 15 mL min⁻¹, and the balance gas was 85 mL min⁻¹ nitrogen (99.99 % purity). The sample were isolated for 30 min to purge the air and keep the apparatus stable and then heated from the room temperature to 1000 °C with the heating rate of 10 °C min⁻¹. The temperature will held constant for 30 min once reached 1000 °C. To obtain the good resolution scanning electron microscope (SEM) figure, the sample was sputter-coated with a thin layer of gold–palladium after mounted on an aluminum stub. XRD (ARL X'TRA, Thermo Scientific, Cu $K\alpha$ radiation) was used to identify minerals and crystallinity. In this study, the XRD data were obtained at an accelerating voltage of 20 kV and a current of 20 mA in the range from 3 to 70° (2-theta) with a scan speed of 0.5° min⁻¹. All the results were analyzed by Jade software. The FT-IR study of functional groups presents in samples was carried out with FT-IR spectrophotometer

(Spectroscopy 100, Perkin-Elmer) by mixing the sample with spectroscopic grade KBr in 1:20 mass ratio. The spectrum was recorded in the wave number region from 400–4000 cm⁻¹ with a resolution of 4 cm⁻¹, and each sample was scan for four times. Mercury intrusion porosimetry is a simple, fast and less costly method for porosity characterization of solid materials. The pore size distribution of fly ash was determined by mercury intrusion porosity (Micrometric Autopore 9500) after the samples were dried at 105 °C for 24 h. The pressure applied in this study was from 0 to 414 Mpa (60,000 psi). Repetition of the tests was done, and the results show good reliability.

Results and discussion

Chemical composition of initial fly ash

The chemical composition of fly ash was first studied by Davis and Carlson in 1937 [21]. The major chemical compositions of fly ash were generally analyzed using X-ray fluorescence (XRF) according to the standard method GB/T 14506.28-2010. In this study, the major compositions of selected ash were analyzed by XRF, and the result is listed in Table 1. The primary components are silica (SiO₂), alumina (Al₂O₃) and iron oxides (Fe₂O₃), with generally lesser content of calcium (CaO), magnesium (MgO), potassium (K₂O) and sodium (Na₂O). According to the classification by ASTM C618, the used fly ash can be designated as class F as the sum content of SiO₂ and Al₂O₃, Fe₂O₃ is greater than 70 %, and the content of CaO is less than 5 %; this kind of fly ash exhibited lower CaO content has been widely explored to be a replacement of Portland cement in mortar [22]; meanwhile, the expansion of concrete will be decreased due to the reduction in alkali ions on the pore solution [23, 24].

Microstructural analysis

Figure 1a, the SEM image of fresh fly ash, shows that most fresh fly ash particles are spherical in shape after the high-temperature combustion process. Its average size was about

Table 1 Chemical composition of coal fly ash (wt%)

Fly ash						
Fe ₂ O ₃	MnO ₂	TiO ₂	CaO	K ₂ O	SO ₃	Σ
17.28	0.0471	0.933	3.002	2.53	3.423	87.17
P ₂ O ₅	SiO ₂	Al ₂ O ₃	Na ₂ O	MgO	LOI	
0.113	46.31	10.7	2.48	0.36	8	

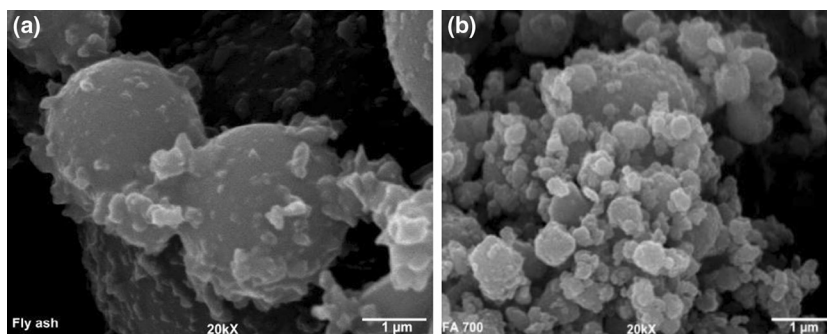


Fig. 1 SEM image of coal fly ash (**a** raw fly ash. **b** ball-mill-treated fly ash)

5 μm , which agree well with the previous report [17]. On the surface of the regular spherical ash particle, there were some smaller irregular fly ash particles, which were likely derived from the high content of iron oxide [25]. The image of the ball-milled fly ash is shown in Fig. 1b. The fly ash particles were clearly crushed, and their shapes were irregular. The sizes of ball-milled fly ash were greatly reduced to about 300 nm, indicating the breakdown of the original spherical-shape fly ash.

Pore structure of coal fly ash

The results of the total intrusion volume, average pore diameter and specific surface area of fly ash samples, shown in Fig. 2, presented the great changes of those parameters with the ball-mill time. The total intrusion volume and average pore diameter decreased sharply as the milling time was increased and exhibited small peak when the ball mill time is around 700 min, which means strong mechanical crushing has been happened during this stage. For the specific surface area, it should be noted that the pore area increased with the milling time and reach highest value at 700 min.

The pore size distribution of samples is shown in Fig. 2, while the raw fly ash has big pores with the diameter larger than 25 nm and can be classified as macropores according to the International Union of Pure and Applied Chemistry (IUPAC) system [26]. It can be seen that as the milling time increases, the milled fly ash significantly increased the specific surface area comparing with the raw fly ash, and the highest value is present at 700 min. At the first stage of short time milling, the cumulative mercury intrusion curve shifted toward smaller pores and lies on the finer side, indicating the formation of small pore. As for the longtime milling, the curve shifted to a larger pores, presenting bigger pores, this may be due to the aggregation effect of long milling time.

FT-IR analysis

Fourier transform infrared (FTIR) was used to obtain the qualitative information about the functional groups of fly ash samples, and the spectra are shown in Fig. 3. The most intense peak of all the tested samples in the spectra occurs around 1000 cm^{-1} , corresponding to Si–O–T (T: Si or Al) stretch vibrations [27], mainly corresponding to silica oxide and aluminum oxide. This result was consistent to that of the XRF analysis of same fly ash sample. Typical bands that appear between 3500 and 3400 cm^{-1} are assigned to the Si–OH bending and stretching of absorbed water on the surface of fly ash samples. A small peak at 1640 cm^{-1} in the spectra is attributed to the bending mode of ($\delta\text{O-H}$) water molecule [28]. The band at 2322 cm^{-1} was observed due to the sorption of carbon dioxide from the air, according to the study of Algoufi and Hameed [29]. The presence of carbonated phase as evidenced by the peak at 1440 cm^{-1} [30]. The small band that presents around 797 cm^{-1} is attributed to the stretching of AlO_4 (condensed), SiO_4 (rings) and amorphous aluminosilicate containing ring structures according to the previous studies [31–33].

The FTIR spectra also clearly show differences of the fly ash samples before and after the ball-mill treatment. Band around 3500 and 3400 cm^{-1} of the ball-milled fly ash indicated an increasing intensity of OH– stretching vibration, contrasting to no appearance of such peak in raw fly ash sample. The formation and presence of Si–OH was an evidence for the breaking down of the silica structure according to the study of Paul et al. [34]. Khalil [35] repeatedly found the appearance of Si–OH in oil palm ash after high-energy ball milling for 30 h, and Patil and Anandhan [36] similarly reported an increase in the peak intensity of Si–OH groups in the ball-milled fly ash for 60 h. Other study indicated that the increased amorphous silica and surface exposure would result in the intense band

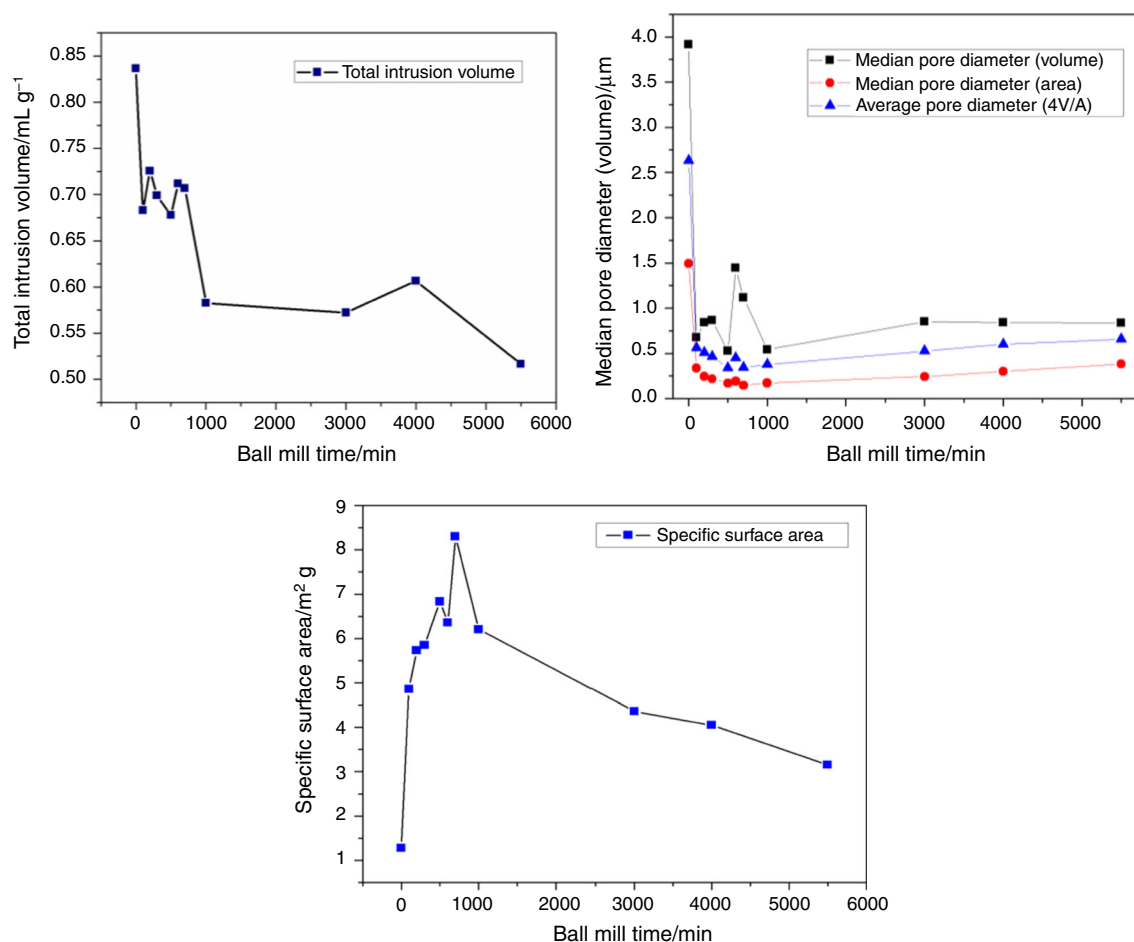


Fig. 2 Distribution of pore volume, pore area and pore diameter for different fly ashes

in this range [37]. However, this peak disappeared when the ball milling time was more than 2000 min. This presented major changes of chemical properties of the ball-milled before the ball-milling time at 2000 min for the selected fly ash sample.

The intensity of FTIR peak at a range of 1300–900 cm^{-1} increased as the ball milling time increased, and this can be interpreted by the increased amorphous silica in the fly ash samples. The peak of Si–O–Si appeared at 1000 cm^{-1} shifted to lower frequencies after ball mill and varied from 1007 to 975 cm^{-1} . This can be interpreted by the Al penetration into the $(\text{SiO}_4)^{4-}$.

Thermogravimetric characteristics of fly ash

Thermogravimetric analysis (TG) was used to determine the thermal stability of the sample by measure the mass loss on heating [38, 39]. The thermogravimetric analysis curves of fly ash under N_2 atmosphere are shown in Fig. 3. A gradual mass loss of 1.3 % occurs from 50 to 200 °C, which may be the result of moisture in the sample. From

400 to 600 °C, small mass loss was recorded indicating volatile matter released in this zone, and for the high temperature of 850–100 °C, the mass loss may due to the presence of the unburn carbon and CaSO_4 in fly ash [40–42].

TG of the fly ashes with different ball-milling time is shown in Fig. 4; obviously, the curves for treated fly ashes with short milling time were located below the raw fly ash, indicating a bigger mass loss compared to the raw fly ash sample, and the main different was occur in the first heat stage. Furthermore, the mass loss is proportional to the ball-milling time and reaches maximum value of 12 %, when the ball-milling time was 700 min, and this may be attributed to the following reaction [43, 44]:



The amount of Si–OH was increased with the ball-milling time, and more H_2O was released when the temperature increased; study of Ul Haq [43] also shows the similar result when the fly ash heated at 65 °C for 72 h, and the Si–OH bonds will transformed to Si–O–T (T: Si or Al) form,

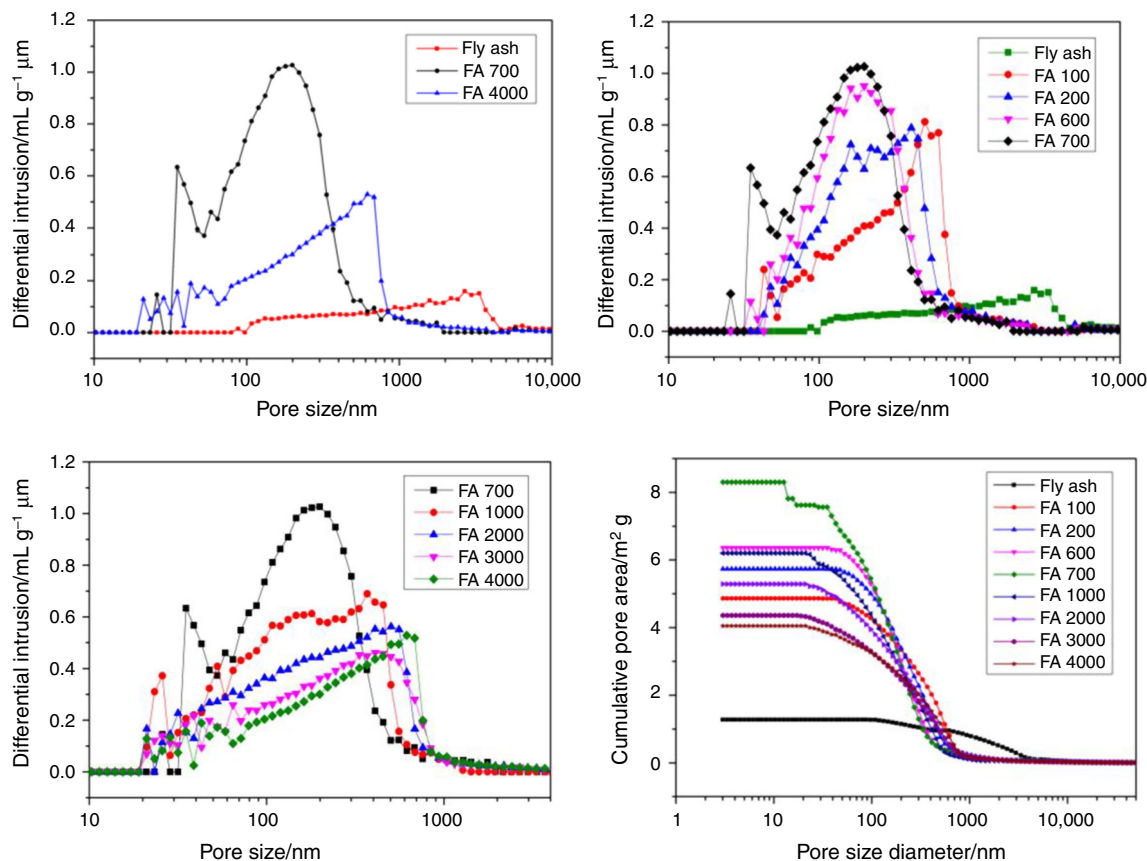


Fig. 3 Pore size distribution of fly ashes with different ball-mill time

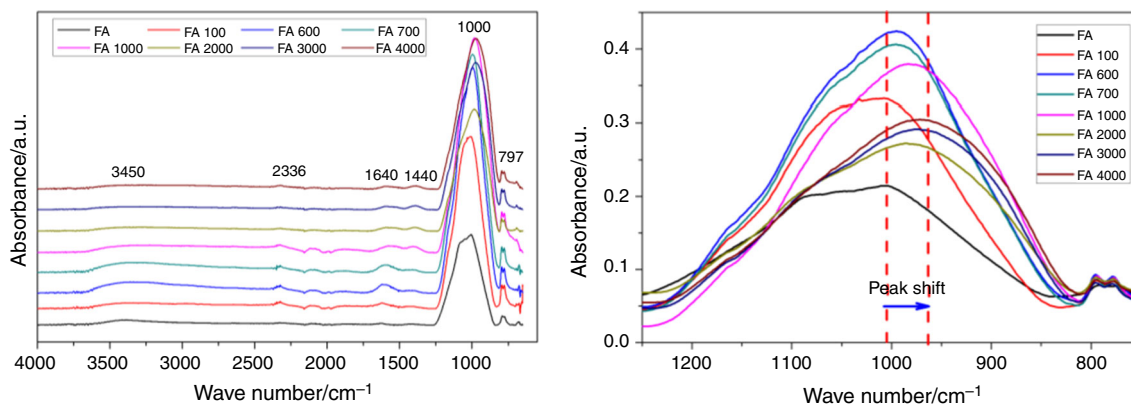


Fig. 4 FTIR spectrum of fly ash with different milling time

thus leading to a higher connectivity, strength and stability. However, as the billing increased to more than 1000 min, the ashes show less mass loss and high thermal stability.

XRD analysis

The XRD patterns of select ball-milled fly ash samples, including the raw fly ash, are shown in Fig. 5. In the raw fly

ash sample, there were a number of crystalline peaks and also an hump of amorphous peak in the diffraction pattern approximately from 15° to 35° (2θ), suggesting the presence of relatively amount amorphous glassy materials. The major crystalline phases of all fly ash samples were identified as quartz, hematite and magnetite in majority, and calcite and mullite in minor. This was well consistent with the results of the XRF analysis. After the ball milling,

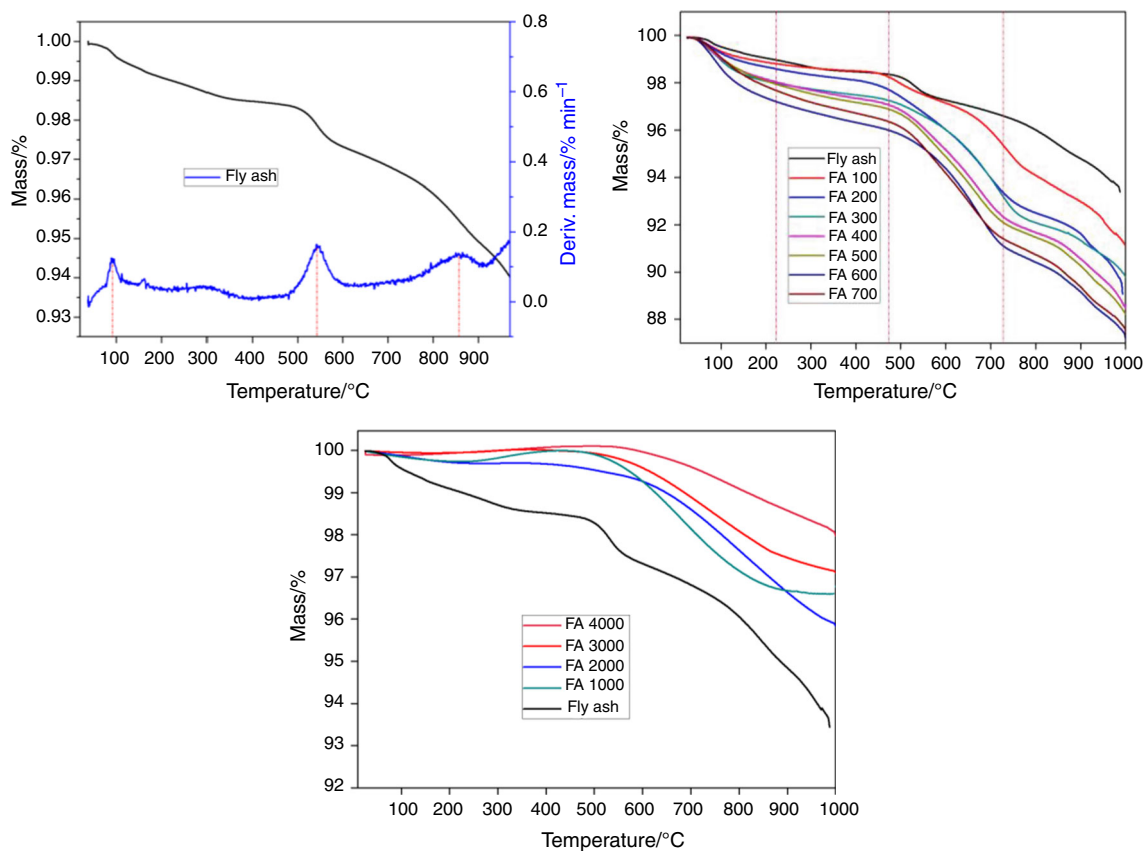


Fig. 5 TG curves for fly ash samples with different milling time

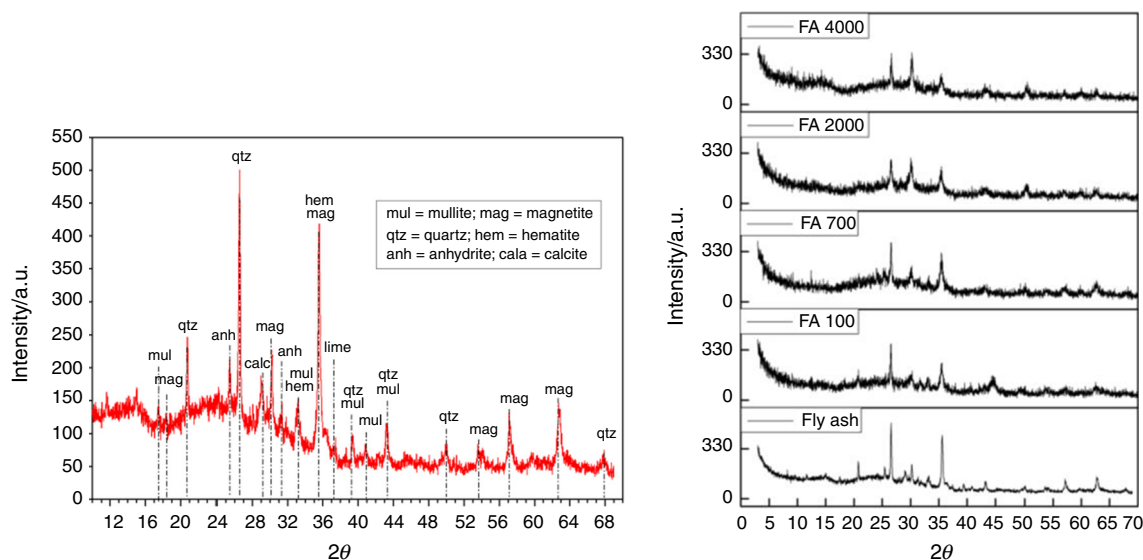


Fig. 6 XRD diffractograms of fly ash samples with different milling time

similar XRD pattern can be observed, but the peak intensities of most original crystallinities significantly diminished and peaks were also broaden. This can be interpreted by the smaller particle size and less extent of crystallinity. The further extension of the ball-milling time from 2000 to

4000 min did not lead any big changes of peak intensities and widths (Fig. 6).

The average crystallite size of the samples was calculated based on the full width at half maximum (FWHM) of the XRD peak according to Scherrer's equation [45].

$$d = \frac{K\lambda}{B \cos \theta} \quad (2)$$

where d is the average grain size, K is the crystallite shape constant (0.89 was used in this study), λ represents the wavelength of Cu $K\alpha$ radiation ($\lambda = 0.1542$ nm), B is the half width of the diffraction peak (FWHM) and θ is the incident angle (25.367°) of X-ray surface [46].

The estimated size of the raw fly ash was 46 nm. After the ball-milling process, the crystallite size decreased to 20 nm, and this change indicated the enhanced amorphous content in fly ash that will be better compatibility [34]. At the first stage of ball milling, dispersion is the main process and results in the sharp decrease in crystallite size, while when the ball-mill time is higher than ~ 2500 min, the size increased due to the effect of aggregation [47].

Conclusions

In the present study, we observed the several major physical and chemical changes of milled fly ash during the high-energy ball-milling process. Significantly, large particles of the original fly ash, regularly in an average of 5 μm , were broke down into much smaller particles, in an average particle size of about 300 nm. The pore structure was also greatly changed by the ball-milling treatment, most big pores disappear, and smaller pores created, showing a close relevant to the milling time. The intensity of –OH stretching vibration peak in FTIR pattern of the ball-milled fly ash had a clear increase with the ball-milling time, but diminished as the milling time was further increased. This was also evidenced by TG results. A long ball-milling time lead the decrease in peak intensity of crystalline phases of the milled fly ash, but the increase in the half width of crystalline peaks, implying more amorphousness and likely a higher reactivity of the ball-milled fly ash toward more applicable utilization.

Acknowledgements This work was supported by the Kentucky Energy and Environment Cabinet (KEEC) Research Funds under contracts of the term 2014–2015, PON 21271300002875, the President Youth Innovation Fund of Anhui Academic of Agricultural Science (14B1354) and US Department of Agriculture (6445-12630-003-00D). The authors also thank China Scholarship Council for the financial support.

Compliance with ethical standards

Conflict of interest None.

References

- James SL, Friščić T. Mechanochemistry: a web themed issue. *Chem Commun*. 2013;49(47):5349–50.
- Suryanarayana C. Mechanical alloying and milling. *Prog Mater Sci*. 2001;46(1–2):1–184.
- Trudeau M, Schulz R, Dussault D, Van Neste A. Structural changes during high-energy ball milling of iron-based amorphous alloys: Is high-energy ball milling equivalent to a thermal process? *Phys Rev Lett*. 1990;64(1):99.
- Fecht H, Hellstern E, Fu Z, Johnson W. Nanocrystalline metals prepared by high-energy ball milling. *Metall Trans A*. 1990; 21(9):2333–7.
- Heidrich C, Feuerborn H, Weir A, editors. Coal combustion products: a global perspective. In: World coal ash WOCA conference, Lexington, KY; 2013.
- Mukherjee AB, Zevenhoven R, Bhattacharya P, Sajwan KS, Kikuchi R. Mercury flow via coal and coal utilization by-products: a global perspective. *Resour Conserv Recycl*. 2008;52(4): 571–91.
- Fisher GL. Biomedically relevant chemical and physical properties of coal combustion products. *Environ Health Perspect*. 1983;47:189.
- Zyryanov VV, Zyryanov DV. Complex processing of pulverized fly ash by dry separation methods. *J Environ Prot*. 2010;1: 293–301.
- Yao ZT, Ji XS, Sarker PK, Tang JH, Ge LQ, Xia MS, et al. A comprehensive review on the applications of coal fly ash. *Earth Sci Rev*. 2015;141:105–21.
- Ahmaruzzaman M. A review on the utilization of fly ash. *Prog Energy Combust Sci*. 2010;36(3):327–63.
- Jala S, Goyal D. Fly ash as a soil ameliorant for improving crop production—a review. *Bioresour Technol*. 2006;97(9):1136–47.
- Basu M, Pande M, Bhadoria P, Mahapatra S. Potential fly-ash utilization in agriculture: a global review. *Prog Nat Sci*. 2009; 19(10):1173–86.
- Liu S, Kong Y, Wang L. A comparison of hydration properties of cement-low quality fly ash binder and cement–limestone powder binder. *J Therm Anal Calorim*. 2014;116(2):937–43.
- Helble J. Trace element behavior during coal combustion: results of a laboratory study. *Fuel Process Technol*. 1994;39(1): 159–72.
- Hurley JP, Schobert HH. Ash formation during pulverized sub-bituminous coal combustion. 1. Characterization of coals, and inorganic transformations during early stages of burnout. *Energy Fuels*. 1992;6(1):47–58.
- Liu G, Zhang H, Gao L, Zheng L, Peng Z. Petrological and mineralogical characterizations and chemical composition of coal ashes from power plants in Yanzhou mining district, China. *Fuel Process Technol*. 2004;85(15):1635–46.
- Li H, Liu G, Cao Y. Content and distribution of trace elements and polycyclic aromatic hydrocarbons in fly ash from a coal-fired CHP plant. *Aerosol Air Qual Res*. 2014;14:1179–88.
- Song C, Xu D, Jiang C, Teng Y, Sun Z, Xu H, et al. The effect of particle size and metal contents on arsenic distribution in coal-fired fly ash. *J Therm Anal Calorim*. 2014;116(3): 1279–84.
- Nomura Y, Fujiwara K, Takada M, Nakai S, Hosomi M. Lead immobilization in mechanochemical fly ash recycling. *J Mater Cycles Waste Manage*. 2008;10(1):14–8.
- Guo X, Xiang D, Duan G, Mou P. A review of mechanochemistry applications in waste management. *Waste Manag*. 2010;30(1): 4–10.
- Davis RE, Carlson RW, Kelly JW, Davis HE. Properties of cements and concretes containing fly ash. In: ACI journal proceedings: ACI; 1937.
- Yilmaz B, Olgun A. Studies on cement and mortar containing low-calcium fly ash, limestone, and dolomitic limestone. *Cement Concr Compos*. 2008;30(3):194–201.
- Shehata MH, Thomas MD. The effect of fly ash composition on the expansion of concrete due to alkali–silica reaction. *Cem Concr Res*. 2000;30(7):1063–72.

24. Tsimas S, Moutsatsou-Tsima A. High-calcium fly ash as the fourth constituent in concrete: problems, solutions and perspectives. *Cement Concr Compos.* 2005;27(2):231–7.
25. Bhattacharjee A, Mandal H, Roy M, Kusz J, Hofmeister W. Physical characteristics of fly ashes from three thermal power plants in West Bengal, India: a comparative study. *Int J Chem Tech Res.* 2013;5:836–43.
26. Everett D. Manual of symbols and terminology for physico-chemical quantities and units, Appendix II: definitions, terminology and symbols in colloid and surface chemistry. *Pure Appl Chem.* 1972;31(4):577–638.
27. Huang Y, Han M. The influence of α -Al₂O₃ addition on microstructure, mechanical and formaldehyde adsorption properties of fly ash-based geopolymer products. *J Hazard Mater.* 2011;193:90–4.
28. Kiseler A, Lygin V. Infrared spectra of surface compounds and adsorbed substances. Moscow: Nauka; 1992.
29. Algoufi YT, Hameed BH. Synthesis of glycerol carbonate by transesterification of glycerol with dimethyl carbonate over K-zeolite derived from coal fly ash. *Fuel Process Technol.* 2014; 126:5–11.
30. Nakamoto K. Infrared and Raman spectra of inorganic and coordination compounds. Hoboken: Wiley Online Library; 1978.
31. Lee W, Van Deventer J. Structural reorganisation of class F fly ash in alkaline silicate solutions. *Colloids Surf A.* 2002;211(1): 49–66.
32. Zhang Y, Sun W, Chen Q, Chen L. Synthesis and heavy metal immobilization behaviors of slag based geopolymer. *J Hazard Mater.* 2007;143(1–2):206–13.
33. Li Z, Liu S. Influence of slag as additive on compressive strength of fly ash-based geopolymer. *J Mater Civ Eng.* 2007;19(6):470–4.
34. Paul KT, Satpathy S, Manna I, Chakraborty K, Nando G. Preparation and characterization of nano structured materials from fly ash: a waste from thermal power stations, by high energy ball milling. *Nanoscale Res Lett.* 2007;2(8):397–404.
35. Khalil HA, Fizree H, Jawaid M, Alattas OS. Preparation and characterization of nanostructured materials from oil palm ash: a bioagricultural waste from oil palm mill. *BioResources.* 2011; 6(4):4537–46.
36. Patil AG, Anandhan S. Ball milling of class-F Indian fly ash obtained from a thermal power station. *Int J Energy Eng.* 2012; 2(2):57–62.
37. Khatri C, Rani A. Synthesis of a nano-crystalline solid acid catalyst from fly ash and its catalytic performance. *Fuel.* 2008; 87(13–14):2886–92.
38. Nocuń-Wczelik W, Łagosz A, Kowalski B, Gawlicki M. Calorimetry in testing waste materials from the brown coal combustion. *J Therm Anal Calorim.* 2014;118(1):123–31.
39. Febrero L, Granada E, Pérez C, Patiño D, Arce E. Characterisation and comparison of biomass ashes with different thermal histories using TG-DSC. *J Therm Anal Calorim.* 2014;118(2): 669–80.
40. Huang Y, Wang S, Hou P, Chen Y, Gong C, Lu L. Mechanisms and kinetics of the decomposition of calcium barium sulfoaluminate. *J Therm Anal Calorim.* 2015;119(3):1731–7.
41. Pacewska B, Nowacka M. Studies of conversion progress of calcium aluminate cement hydrates by thermal analysis method. *J Therm Anal Calorim.* 2014;117(2):653–60.
42. Fan M, Brown RC. Comparison of the loss-on-ignition and thermogravimetric analysis techniques in measuring unburned carbon in coal fly ash. *Energy Fuels.* 2001;15(6): 1414–7.
43. Ul Haq E, Padmanabhan SK, Licciulli A. Synthesis and characteristics of fly ash and bottom ash based geopolymers—a comparative study. *Ceram Int.* 2014;40(2):2965–71.
44. Li Q, Xu H, Li F, Li P, Shen L, Zhai J. Synthesis of geopolymer composites from blends of CFBC fly and bottom ashes. *Fuel.* 2012;97:366–72.
45. Borchert H, Shevchenko EV, Robert A, Mekis I, Kornowski A, Grübel G, et al. Determination of nanocrystal sizes: a comparison of TEM, SAXS, and XRD studies of highly monodisperse CoPt₃ particles. *Langmuir.* 2005;21(5):1931–6.
46. Stock S, Cullity B. Elements of X-ray diffraction. Upper Saddle River: Prentice Hall; 2001.
47. Fadda S, Cincotti A, Concas A, Pisu M, Cao G. Modelling breakage and reagglomeration during fine dry grinding in ball milling devices. *Powder Technol.* 2009;194(3):207–16.